Magnon-drag and field-direction dependent thermopower in low-damping ferromagnetic Co$_{25}$Fe$_{75}$ alloy thin films

M. R. Natale, D. J. Wesenberg, and B. L. Zink ●*

Department of Physics and Astronomy, University of Denver, Denver, Colorado 80208, USA

Recent experimental and theoretical work has focused new interest on magnon contributions to transport properties of metallic ferromagnets. Here we present the Seebeck coefficient, or thermopower, measured from 78 to 325 K for Co$_x$Fe$_{1-x}$ thin films and discuss the role of the Gilbert damping parameter, α_{GD}, on electron-magnon interactions. These measurements are made with micromachined Si-N thermal isolation platforms that allow excellent control of the thermal gradient applied to a thin film. We first present zero-field measurements of the absolute Seebeck coefficient, α_{abs}, for two films with $x = 0.25$, the alloy composition previously shown to have low damping and long-lived spin excitations, and a third film with $x = 50$ where α_{GD} is higher, and more typical of other 3D alloy ferromagnets. We compare these to pure Co and Fe films, and to simple expectations from the electronic DOS. This indicates that a large additional thermopower appears where spin excitations are long-lived. This additional zero-field thermopower can be explained by magnon drag, where momentum is transferred from thermal, exchange-dominated magnons to the electron system. We then present the dependence of the thermopower on the direction of an applied in-plane magnetic field. Comparison of this magnetothermopower (MTP) to anisotropic magnetoresistance (AMR) measured via four-wire electrical resistance measured on the same films shows, as in previous measurements of thermal conductivity in the same samples, a field-direction dependent contribution to thermopower. The MTP also allows improved estimation of the electronic diffusion thermopower, which then allows us to construct a plausible model for the zero-field thermopower of the low-damping films that adds the theoretically predicted magnon drag, and matches measured α_{abs} well at low T. The field-direction dependent contribution, not previously observed, also suggests interaction of electrons with the lower wave-vector dipole or dipole-exchange dominated magnetostatic spin waves, which is an alternate manifestation of magnon drag.

I. INTRODUCTION

Interactions between charge, thermal gradients and internal magnetization textures have played a significant role in the development of spintronics [1–3] and spin caloritronics [4–8] in recent years. Electrical and thermal transport properties of thin film FM alloys play a key role in spintronics and spin caloritronics, and are currently being reexamined after theoretical [9–16] and experimental [12,17–21] work has shown that magnons (or spin waves), the fundamental excitation of an ordered magnetic ground state, can play a role. Magnon effects are particularly interesting when these spin dynamics can be long-lived. This lifetime is usually limited by either magnon-electron scattering events, primarily from [s-d] exchange, τ_{sd}, or by magnon-phonon scattering. Understanding of the magnon or spin wave lifetime in a given material is usually gained from FMR measurements of the Gilbert damping parameter, α_{GD}. The materials with the lowest α_{GD} are usually insulators such as yttrium iron garnet [22,23], due to a near absence of conduction electrons. However, recent work has shown that tuning the alloy composition in BCC Co-Fe alloys results in much lower Gilbert damping than seen in typical metallic ferromagnets [24,25]. In these reports, a minimum in the density of states, $n(E_F)$, at the Fermi level corresponds to a minimum of α_{GD} at Co concentration of approximately 25%. The damping parameter for this Co$_{25}$Fe$_{75}$ alloy has been reported in the range $\alpha_{GD} \cong 10^{-3}–10^{-4}$, comparable to the FM insulator yttrium iron garnet with $\alpha_{GD} \cong 10^{-4}–10^{-5}$ for similar film thicknesses [22,26–28]. Furthermore, Brillouin light scattering (BLS) microscopy experiments have demonstrated that spin-wave propagation lengths in ultra-low-damping Co$_{25}$Fe$_{75}$ thin films can reach tens of micrometers at room temperature, making them useful for metallic magnonic applications [25,29].

In our previous work on Co$_x$Fe$_{1-x}$ thin films, we reported a nonelectronic contribution to thermal conductivity based on deviation from the Wiedemann-Franz law in Co$_{25}$Fe$_{75}$ that is absent in Co$_{50}$Fe$_{50}$. We argued that this contribution is likely to be magnonic in nature, based partly on field-direction dependent measurements of thermal conductivity [21]. As a possible explanation for this field-direction dependence, we considered the differing transport of the $H \parallel \nabla T$ backward-volume spin waves (BVSW) and the $H \perp \nabla T$ Damon-Eshbach spin waves (DESW) or magnetostatic spin waves (MSSW) [30,31]. A simple model based on the dispersion relationships of these field-direction dependent modes could plausibly explain the magnitude of the field-direction

---

*barry.zink@du.edu

dependence of k [21]. In this paper, we report electrical resistivity and thermopower, or Seebeck coefficient, measured on the same films as used for the thermal conductivity study. We report an enhanced thermopower in $Co_{25}Fe_{75}$ that is much larger than the electronic diffusion thermopower predicted by the Mott equation. As was previously reported for bulk Co-Fe alloys [20], we associate this additional thermopower with magnon drag. As with the thermal conductivity, the higher damping $Co_{50}Fe_{50}$ alloy film shows smaller thermopower values that are better explained by diffusion thermopower, indicating low or nonexistent magnon drag. We also present field-dependent measurements that compare resistance, $R(H)$, and thermopower, $\alpha_{abs}(H)$. A unique field-dependence of the Seebeck coefficient in the low-damping $x = 25$ alloy, not apparent in the $x = 50$ sample, is similar to the field-orientation dependence of k, and indicates a previously unknown manifestation of magnon drag, likely caused by momentum transfer from magnetostatic spin waves to the conduction electrons.

II. BACKGROUND AND THEORY

The presence of a thermal gradient causes electrons in metals to diffuse from the hot to the cold end. This establishes an electric field and a subsequent potential difference, or Seebeck voltage, ΔV. The thermopower, or Seebeck coefficient α, under certain assumptions regarding the direction of the thermal gradient and the measurement circuit [32], is given by $\alpha = \Delta V / \Delta T$, where ΔT is the temperature difference from hot to cold. This diffusive electronic thermopower is calculated using the Mott relation, α_{Mott}, given by [33,34]

$$\alpha_{Mott} = -\frac{\pi^2 k_B^2 T}{3e} \frac{1}{\rho(E)} \left[\frac{\partial \rho(E)}{\partial E} \right]_{E=E_F}, \quad (1)$$

where ρ is the electrical resistivity, E_F is the energy at the Fermi level, k_B is the Boltzmann constant, T is temperature, e the charge of the carrier, and $[\partial \rho / \partial E]|_{E_F}$ is the energy derivative of the resistivity evaluated at the Fermi energy.

Applying a thermal gradient to FM metals can also excite spin dynamics, resulting in nonequilibrium conditions where magnon heat carriers can impart momentum to electrons, adding to the thermopower. In analogy to phonon drag, where phonons flowing in response to the thermal gradient can transfer momentum to the electrons and add to thermopower, this contribution to thermopower is termed magnon drag [9,13,18,20], as shown schematically in Fig. 1(a). Magnon drag has been observed in both elemental and alloy transition metal FM thin films [18,35,36] and complex FM oxides [37]. However, quantitative and accurate identification of magnon drag is often challenging since the electronic diffusion contribution is not simple to determine. This is obvious from Eq. (1), which depends on $[\partial \rho / \partial E]|_{E_F}$, a quantity not possible to directly measure.

Two theories have been proposed to explain the magnon-drag contribution to thermopower, α_{md}; one built from the classical hydrodynamic model [14,17,18], and the second using a relativistic Landau-Lifshitz-Gilbert (LLG) formalism [9,13,14] to describe the time-varying magnetization. In the hydrodynamic model, α_{md} is derived from drift equations where magnons and electrons are treated as two in-
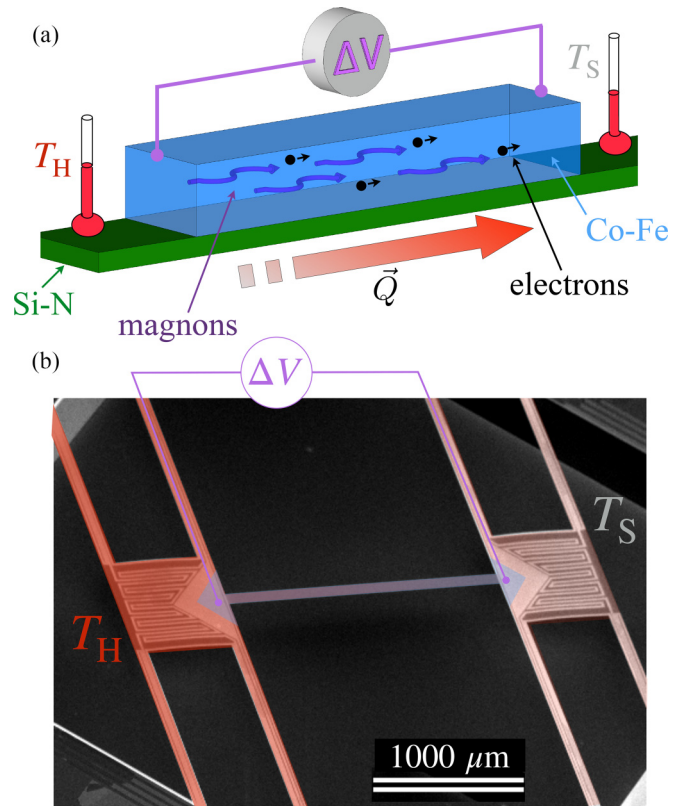

FIG. 1. (a) Schematic view of the thermopower measurement of a low-damping metallic ferromagnet thin film on a suspended Si-N membrane platform with magnon drag. Heat $\vec{Q}$ moves from the heated end of the sample at T_H to the cooler end at T_S. The thermal gradient drives both electron diffusion, and also generates a flow of magnons (shown schematically as purple arrows). These magnons transfer additional momentum to electrons (shown in black), which increases the thermopower. (b) False-color scanning-electron micrograph of the suspended Si-N membrane thermal isolation platform used to measure thermopower. The red shading schematically indicates the temperature, while the blue highlight shows the sample area. Separate heaters and thermometers are patterned on each Si-N island.

dependent but interacting fluids, with magnonic and electronic chemical potentials, μ_m and μ_e, respectively. In the relativistic theory, based on spin orbit interactions, the mechanism relies on spin motive forces transferring spin angular momentum from conduction electrons to the magnetization. Although microscopically very different, Watzman *et al.* showed that these two theories agree in many situations [18]. Due to its dependence on magnon thermal conductivity, which we have probed experimentally in these films [21], here we focus on the relativistic spin-transfer mechanism.

Lucassen *et al.* used this theory to derive a relation associating the spin transfer torque parameter, β, to the magnon-drag thermopower, α_{md}. Two contributions in the long-wavelength limit are responsible, an adiabatic term related to the Berry-phase force, and a dissipative term associated with β [9,13]. Assuming $\alpha_{GD} < \beta$, α_{md} can be written as

$$\alpha_{md} = \beta^* \frac{\hbar^2 \gamma P}{2|e|M_s D} k_m', \quad (2)$$

where $\beta^* = \beta - 3\alpha_{\mathrm{GD}}$, $\gamma = g_e \mu_B / \hbar$, g_e is the gyromagnetic ratio (≈ 2 for metals), $P = (N_\uparrow - N_\downarrow)/(N_\uparrow + N_\downarrow)$ is the spin polarization where $N_\uparrow$ and $N_\downarrow$ are the density of states at the Fermi level for spin up and down populations, respectively. M_s is the saturation magnetization, D is the spin stiffness constant, and the magnon thermal conductivity at zero electric field is given by $k_m = k'_m + \xi - \sigma\alpha_{\mathrm{ep}}(\alpha_{\mathrm{ep}} + \alpha_{\mathrm{em}})T$. Here ξ, α_{ep}, and α_{em} are drag effects between magnon and electron-phonon heat currents, electron-phonon and electron-magnon contributions to thermopower, respectively [9,13,14]. If drag effects between magnon and electron-phonon heat currents are small and electron-phonon contributions to thermopower are negligible, then we can neglect the last two terms, and write the magnon thermal conductivity as $k'_m \approx k_m$. The correction to β (i.e., $\beta^* = \beta - 3\alpha_{\mathrm{GD}}$) is associated with the Berry-phase force, and is due to electrons dragged from the cold to the hot regions of the thermal gradient [9,13].

The resulting simple theoretical model of thermopower when both electronic diffusion and magnon drag are present is then $\alpha_{\mathrm{theory}} = \alpha_{\mathrm{Mott}} + \alpha_{\mathrm{md}}$.

III. EXPERIMENT

We measure resistivity and the longitudinal thermopower for each sample on micromachined thermal isolation bridge-platform devices consisting of 500 nm of low-stress, amorphous silicon-nitride (Si-N) on $\langle 100 \rangle$ silicon wafers. An example thermal isolation structure is shown in Fig. 1(b). Thermometers, heaters, and electric leads are patterned on each of the two islands by photolithography followed by e-beam evaporation of a 10 nm adhesion layer of Cr and 40 nm of Pt at rates of 0.1 and 0.2 nm/s, respectively. The suspended bridge, with dimensions of 2050 μm × 88 μm, connects the two Si-N islands, which have triangular contact pads that allow voltage and resistance measurement of a film deposited on the bridge. These triangular features also help keep the temperature uniform across each island. The geometry of the device maintains an in-plane heat flux and a unidirectional thermal gradient, which enables accurate thermal measurements [34,38,39].

The $\mathrm{Co_x Fe_{1-x}}$ alloys were cosputtered from separate targets of elemental Co and Fe via DC magnetron sputtering in Ar after reaching chamber pressure of $\cong 4 \times 10^{-8}$ Torr at a rate of 0.25 nm/s on a 3 nm Ti/5 nm Cu seed layer, and capped with a 5 nm Al film to limit oxidation. This follows previously reported thin-film growth techniques to achieve the desired BCC crystal structure for the alloy samples [40,41]. We verified the composition of the $\mathrm{Co_x Fe_{1-x}}$ alloy by x-ray diffraction (XRD) spectroscopy on witness samples grown on Si-N coated Si substrates in the same depositions [24,41]. We also e-beam evaporated 75 nm thick films of Fe and Co in ultrahigh vacuum (UHV) conditions ($\cong 10^{-8}$ to 10^{-10} Torr) at rates approximately 0.1 nm/s to provide pure composition references for the alloyed materials.

We mounted the thermal platforms to a gold-plated copper block, wire bonded to electrical leads and enclosed the sample in a radiation shield. The cryostat is placed under vacuum ($\cong 10^{-6}$ Torr) to minimize convection heating. The film resistance, R, is measured using a four-wire method and the resistivity is calculated by $\rho = R(wt)/l$ where l, w, and t are

the length, width, and thickness of the film, respectively. The longitudinal Seebeck coefficient measurements are made by recording the voltage drop, or thermoelectric voltage (TEV), across the film after applying a unidirectional thermal gradient by Joule heating the heater on one Si-N island. We determine the thermopower from linear fits to a series of measured thermovoltages, ΔV, at several applied temperature differences, ΔT, since when the thermal gradient is uniform and the current path well-defined, $\alpha = \Delta V / \Delta T$. This gives the relative Seebeck coefficient, which includes contribution from the Pt leads. In an earlier paper we presented a method to estimate this lead contribution for our thermal isolation platform [32], and here we subtract this lead contribution (the absolute value of this contribution is $\leqslant 5$ μV/K for all T studied here) and report the absolute Seebeck coefficient of the magnetic thin films. Further details on the measurement techniques and fabrication steps for the thermal isolation platforms can be reviewed in previous reports [32,38,39,42,43].

IV. RESULTS AND DISCUSSION

Figure 2 displays temperature dependence of ρ and α_{abs} over the temperature range 78–325 K for 75 nm thin-films of Co, Fe, and two different $\mathrm{Co_x Fe_{1-x}}$ alloy compositions; $x = 25$ (two different samples labeled #1 and #2) and the $x = 50$ Co composition. In Fig. 2(a), the behavior of ρ for all films is nearly linear with T, as expected for metals. In the 75 nm thick elemental films, $\rho_{\mathrm{Co}} < \rho_{\mathrm{Fe}}$ is in agreement with bulk trends, while both exhibit higher ρ values due to defects, grain boundary and surface scattering as expected for any thin film. Of the two alloy compositions, a higher ρ is observed in the low-damping $\mathrm{Co_{25}Fe_{75}}$, which correlates with the density of states, $n(E_F)$, at the Fermi level. The $x = 50$ alloy exhibits a higher n_{E_F} and correspondingly lower resistivity [41]. We attribute the variation in ρ between samples #1 and #2 films to the small variations in Co concentration and lattice parameters, which we previously determined via XRD and discussed in our previous work [21]. Note for concentrations of 50% Co, the electrical resistivity is similar to elemental Co for temperatures above 200 K.

In Fig. 2(b), the absolute thermopower, α_{abs}, is shown for all films. The Seebeck coefficient for Co, and $\mathrm{Co_{50}Fe_{50}}$ films are approximately linear with T, with only slight deviations observed. The linear response likely indicates that α_{abs} is dominated by electron diffusion, which is described well by Eq. (1), where $\alpha \propto 1/\rho$, assuming minimal temperature variation in the energy derivative of ρ. The α_{abs} of 75 nm Fe thin film is nonlinear, with a broad peak trending to a sign change as T increases. These features in Fe are in line with previous reports on magnon-drag contributions to thermopower [18,20,35]. The two $\mathrm{Co_{25}Fe_{75}}$ films have similar thermopower, and both are the largest negative values seen in this group of samples. The sign and absolute value are both in line with previous measurements of similar alloys in bulk [20]. The differences in the thermopower of the two alloy compositions agrees well with the relationship $n(E_F) \propto \alpha_{\mathrm{GD}}$ [41]. However, from the magnitude of ρ seen in Fig. 2(a), simple application of the Mott equation [Eq. (1)] suggests that the thermopower of the low-damping film $\mathrm{Co_{25}Fe_{75}}$ should be a smaller negative value than $\mathrm{Co_{50}Fe_{50}}$. Instead, $\mathrm{Co_{25}Fe_{75}}$
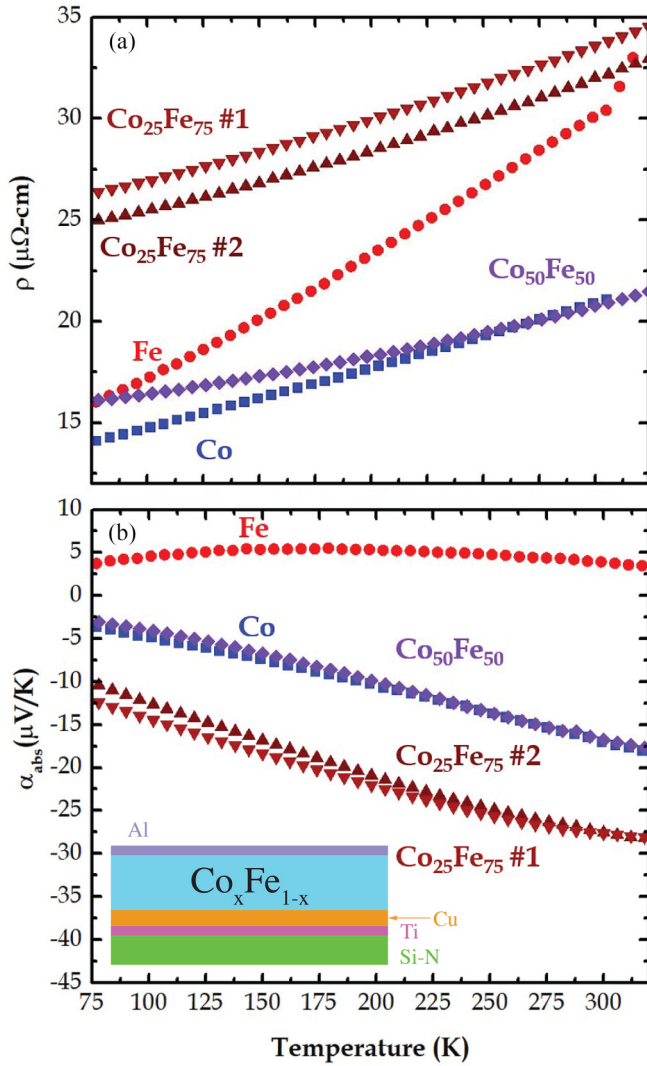
FIG. 2. Temperature dependence of (a) resistivity, ρ, and (b) absolute thermopower, α_{abs}, for 75 nm thick Co, Fe, and three alloy compositions $Co_{25}Fe_{75}$ #1, $Co_{25}Fe_{75}$ #2, and $Co_{50}Fe_{50}$. Inset: Schematic view of the $Co_xFe1 - x$ sample stack with seed and cap layers indicated.

FIG. 3. AMR measurement for samples (a) $Co_{50}Fe_{50}$ and (b) $Co_{25}Fe_{75}$ showing $R(H)$ at 200 K for I parallel and perpendicular to H, denoted on the plot as $H_{\parallel}$ and $H_{\perp}$. Curved arrows indicate the field sweep direction and are color coordinated to help distinguish between $R(H, \parallel, \uparrow)$ (Dark green), $R(H, \parallel, \downarrow)$ (light green), $R(H, \perp, \uparrow)$ (dark blue), and $R(H, \perp, \downarrow)$ (light blue). The estimated error bar shown in panel (a) is calculated by the uncertainty in field, in angle between I and ∇T, and in zero-field resistance values.

shows a larger negative thermopower, while $Co_{50}Fe_{50}$ matches well with the Co thin film. This is the first indication of a significant additional contribution to thermopower in the low-damping sample.

Figure 3 shows field-dependent resistance, $R(H)$, measured at 200 K as a function of external field, H, over the range ± 400 Oe (40 mT). Arrows indicate the direction of the field sweep, starting at and returning to the positive saturated value. To distinguish in-plane field orientation with respect to the applied current, I, the following notation is used; $R(H, \parallel)$ and $R(H, \perp)$. All field measurements are taken over the temperature 125–300 K in increments of 25 K. The results for both $Co_{25}Fe_{75}$ #1 and $Co_{50}Fe_{50}$ alloys are broadly in line with the expectations of anisotropic magnetoresistance (AMR), as has been reported for many ferromagnetic metals and alloys including Co, Fe, Ni, and Py [42,44,45]. In both films, a symmetric field dependence is observed as H sweeps through
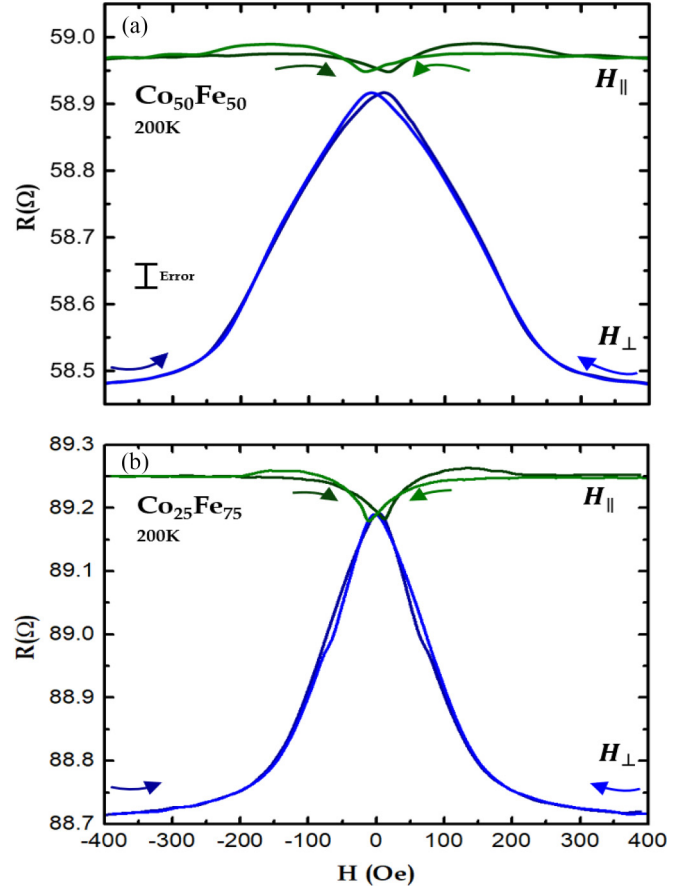
0 due to spin-dependent scattering associated with spin-orbit coupling. For $Co_{50}Fe_{50}$, with a larger α_{GD}, a broader curve in both orientations is observed from 125–300 K, though this most likely indicates a larger coercive field in this alloy. The difference in maximum field values for this alloy, given by $\Delta R(H) = R(H, \parallel) - R(H, \perp)$, is $\cong 0.5$ Ω. The small difference between the R values measured at the coercive field, where the sample magnetization passes through zero and R is often expected to be independent of field direction, are close to our estimated error and likely result from a slight misalignment of this sample during that measurement. The low-damping polycrystalline alloy, $Co_{25}Fe_{75}$, with narrower peaks in both field orientations, shows a similar $\Delta R(H) \cong$ 0.5 Ω. Both films exhibit minute changes with respect to field orientation ($<1\%$) over the entire temperature range. We note that both Co_xFe_{1-x} alloys show a unique behavior, reaching a maximum $R(H, \parallel)$ before plateauing to a steady resistance level. $R(H, \perp)$ also shows a slight inward shift as $H \to 0$ that is more distinguishable in the $x = 25$ sample. These observations, although subtle, are unaccounted for but consistent throughout the temperature range measured.
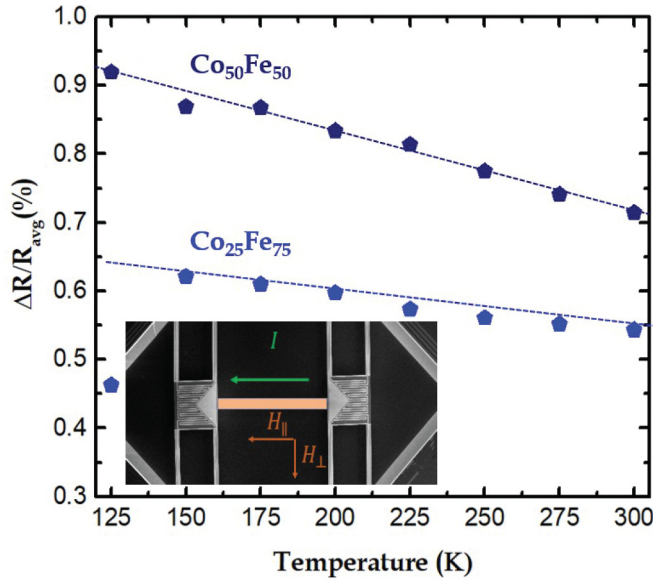
FIG. 4. AMR Ratio for both alloys over the temperature range 125–300 K as calculated using Eq. (3). Inset: SEM image representing orientation between H and I.

The AMR ratio is defined [39,44]

$$\Delta R / R_{\mathrm{avg}} = \frac{R(H, \parallel) - R(H, \perp)}{(1/3)R(H, \parallel) + (2/3)R(H, \perp)}, \qquad (3)$$

where $\Delta R = R(H, \parallel) - R(H, \perp)$ and $R_{\mathrm{avg}} = (1/3)R(H, \parallel) + (2/3)R(H, \perp)$. As shown in Fig. 4, the AMR ratio is consistent with earlier measurements of this alloy, and decreases linearly with respect to temperature above 150 K as expected from increased scattering events. Differences seen between the two alloy films can be attributed to slight differences in spin-orbit coupling parameters (λ_{SO}) between Co and Fe [25,41,46]. Below 125 K, the $x = 25$ sample shows a significant decrease in magnitude which requires further investigation.

We also performed magnetothermopower (MTP) measurements, $\alpha_{\mathrm{abs}}(H)$, in applied field up to ± 400 Oe in both $H \parallel \nabla T$ and $H \perp \nabla T$ orientations. From the relationship between α and ρ shown in Eq. (1), one expects similar field dependence, and indeed in typical transition metal and transition metal alloy films our group and others have observed patterns of MTP that match the magnetoresistance well [39,42,45,47,48]. For the $\mathrm{Co}_x\mathrm{Fe}_{1-x}$ films, with their negative absolute thermopower, the expected pattern would be that when $H \parallel \nabla T$, $\alpha_{\mathrm{abs}}(H, \parallel)$ becomes more negative (increases) as $H \to 0$, before returning to saturated levels. When $H \perp \nabla T$, $\alpha_{\mathrm{abs}}(H, \perp)$ would then be expected to increase to a more positive value (reducing thermopower) as $H \to 0$ until returning to α_{sat} at 400 Oe. As shown in Fig. 5(a), the $x = 50$ film is roughly in line with this pattern, though the field-driven change in α_{abs} was close to our estimated error for this particular experimental run. We define $\Delta \alpha_{\mathrm{sat}} = \alpha_{\mathrm{abs}}(H, \parallel) - \alpha_{\mathrm{abs}}(H, \perp)$ at 400 Oe and determine the magnitude for $\mathrm{Co}_{50}\mathrm{Fe}_{50}, \cong 7.5$ nV/K at 200 K.

As shown in Fig. 5(b), the low-damping $\mathrm{Co}_{25}\mathrm{Fe}_{75}$ film manifests a different and unexpected field-orientation dependence. Here $\alpha_{\mathrm{abs}}(H, \parallel)$ responds as expected with respect to field, however $|\alpha_{\mathrm{abs}}(H, \parallel)| > |\alpha_{\mathrm{abs}}(H, \perp)|$, unlike previous
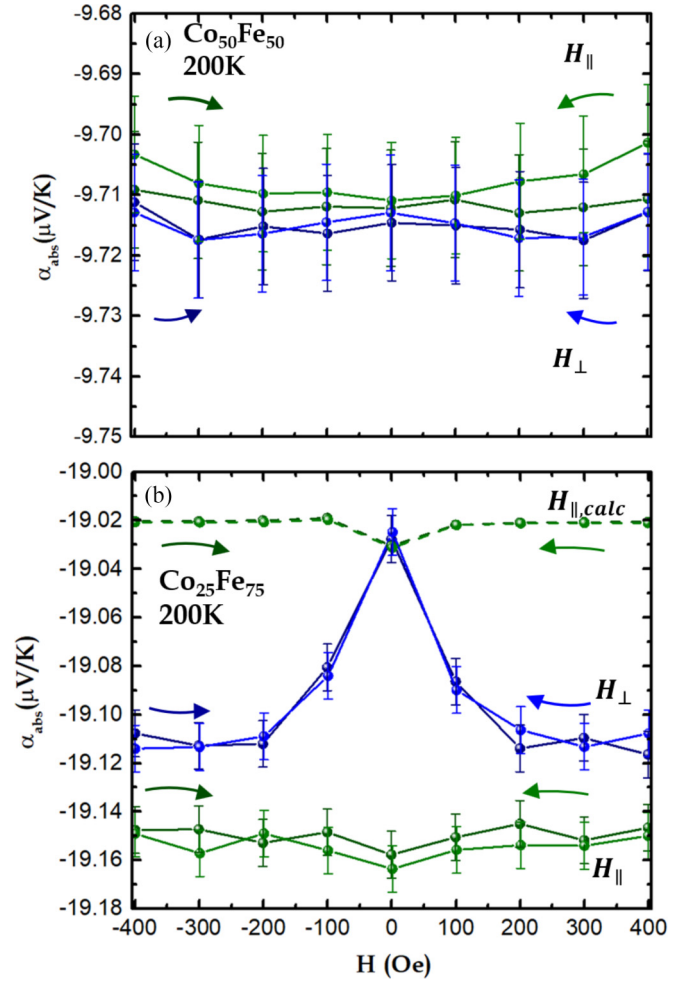

FIG. 5. MTP measurement for samples (a) $\mathrm{Co}_{50}\mathrm{Fe}_{50}$ and (b) $\mathrm{Co}_{25}\mathrm{Fe}_{75}$. $\alpha_{\mathrm{abs}}(H)$ at 200 K for ∇T parallel and perpendicular to H, denoted on the plot as $H_{\parallel}$ and $H_{\perp}$. Curved arrows indicate the field sweep direction and are color coordinated to help distinguish between $\alpha(H, \parallel, \uparrow)$ (Dark green), $\alpha(H, \parallel, \downarrow)$ (light green), $\alpha(H, \perp, \uparrow)$ (dark blue), and $\alpha(H, \perp, \downarrow)$ (light blue). Dotted lines are shown from calculated values using linear relationship $\alpha_{\mathrm{calc}}(H, \parallel) = m(1/R(H, \parallel)) + b$, where m and b are determined at each temperature from measured $\alpha(H, \perp)$ and $R(H, \perp)$ values.

measurements on 3D ferromagnetic alloy thin films [3,39,42]. This suggests that another mechanism could be contributing to thermopower when the field is parallel to the applied thermal gradient, the condition where the same sample showed increased thermal conductivity [21]. As a result, for the $x = 25$ alloy, $\Delta \alpha_{\mathrm{sat}} \cong -130$ nV/K at 200 K. This is much larger, and as highlighted earlier shows the opposite sign compared to $x = 50$. To the best of our knowledge, this pattern of field-dependence has not been reported in previously studied Co-Fe alloys, or in other metallic ferromagnets.

Before turning to additional analysis of this additional field-direction dependent thermopower, we first calculate the magnetothermopower (MTP) ratio, defined in analogy to the AMR ratio by

$$\alpha_{\mathrm{MTP}} = \frac{\alpha_{\mathrm{abs}}(H, \parallel) - \alpha_{\mathrm{abs}}(H, \perp)}{(1/3)\alpha_{\mathrm{abs}}(H, \parallel) + (2/3)\alpha_{\mathrm{abs}}(H, \perp)}, \qquad (4)$$
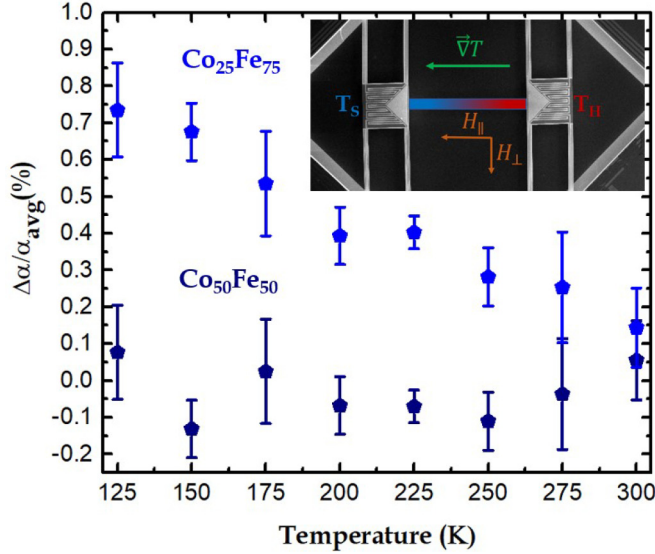
FIG. 6. MTP Ratio for both alloys over the temperature range 125–300 K is calculated using Eq. (4). Inset: SEM image representing orientation between H and ∇T.

where $\alpha(H, \parallel)$, $\alpha(H, \perp)$ show orientation of the external field with respect to ∇T. As shown in Fig. 6, the MTP ratio for the two films are markedly different. $Co_{50}Fe_{50}$ has MTP ratio that remains near 0, within experimental error, a consequence of the small field-dependence observed in $\alpha_{abs}(H)$ versus H throughout the entire temperature range. In contrast, the MTP ratio for the Co-Fe alloy with 25% Co is larger, and decreases in a nearly linear fashion with respect to temperature, trending from approximately 0.8% at 125 K to near 0 at room temperature. This behavior agrees well with the trend of $k_m \to 0$ for the same low-damping film for in our previous report [21].

We begin a closer analysis of the field-dependent shift in α_{abs} in the $x = 0.25$ sample with a closer look at the near-zero field behavior. Measurements of α_{abs} as a function of field are challenging in part since the series of applied thermal gradients we typically employ to most accurately remove contributions from leads and other artifacts can make the measurement long enough that thermal and other longer-term drift can add uncertainty. In Fig. 7 we aim to more carefully map the low field variation in thermopower by cycling the heater current between 0 and 110 μA, using a single thermal gradient to more rapidly sweep the field in finer steps [49]. This allows a closer examination of the thermovoltage, ΔV, in each orientation near zero applied field, where in the simplest picture one would expect both R and α_{abs} to be independent of field direction. Figure 7(a) shows ΔV versus H at 150 K, with the field swept from $\pm$ 400 Oe in both orientations. The zero-field values remain different, and still agree well for each sweep direction. This could indicate that the field steps used still missed the true zero due to expected slight field measurement offsets, as shown in the inset to Fig. 7(a). It is more likely that the domain state at zero applied field is different after saturation in different field directions. We observed a similar effect for thermal conductivity in these samples [21]. While transport properties such as resistance or thermopower often have the same value when the internal
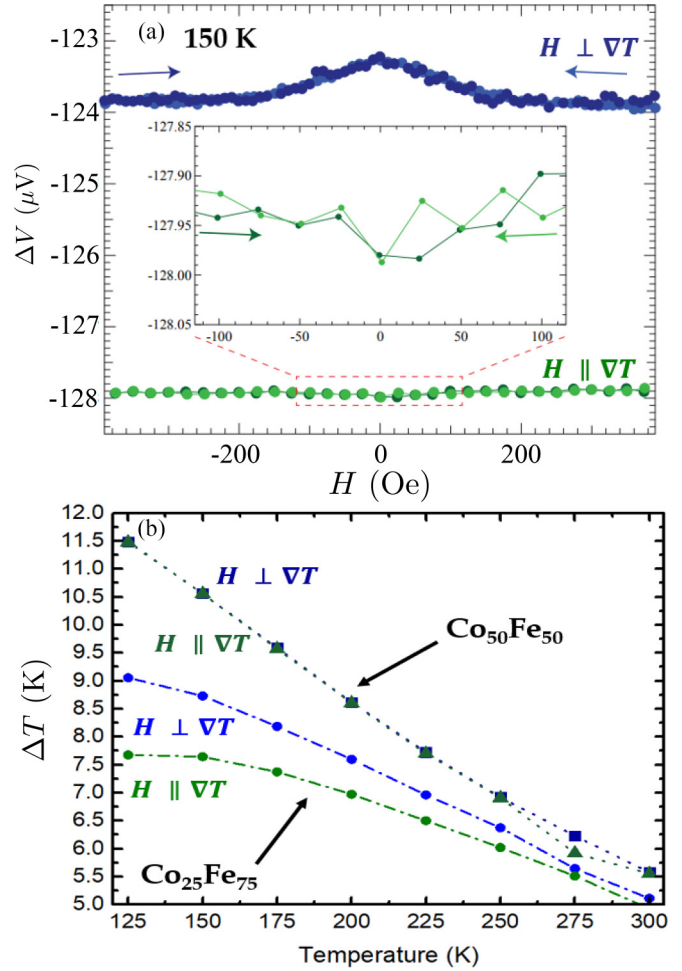

FIG. 7. (a) Thermovoltage, ΔV for a single heater current = 110 μA at 150 K for ∇T parallel and perpendicular to H, denoted on the plot as $H_\parallel$ and $H_\perp$. Arrows indicate the field sweep direction and are color coordinated to help distinguish between $\alpha(H, \parallel, \uparrow)$ (Dark green), $\alpha(H, \parallel, \downarrow)$ (light green), $\alpha(H, \perp, \uparrow)$ (dark blue), and $\alpha(H, \perp, \downarrow)$ (light blue). (b) Applied temperature differences for samples $Co_{50}Fe_{50}$, and $Co_{25}Fe_{75}$ at saturating fields of 400 Oe over the temperature range of 125–300 K.

field in the sample is zero, this is not always the case. For example, there are many well documented cases of the resistance depending on the details of the zero-field domain pattern that forms in a thin film or nanowire, which can be different after the sample is saturated in different directions [50–54]. It is interesting, however, that the resistance of the $x = 0.25$ film, as seen in Fig. 3(b), is insensitive to any difference in the domain pattern formed after saturation in different directions, while k and α are affected by this altered magnetic texture. Figure 7(b) shows the measured temperature dependence ΔT across the bridge resulting from the 110 μA heater current applied at saturating field of 400 Oe in each orientation for both Co_xFe_{1-x} films. This value is determined using the separate, calibrated Pt thermometers at each end of the sample bridge, and restates the results of our earlier investigation of thermal conductivity. We see higher ∇T and no dependence on field direction for the $x = 50$ film, and lower ∇T with strong dependence on field direction for the $x = 25$ film. Since
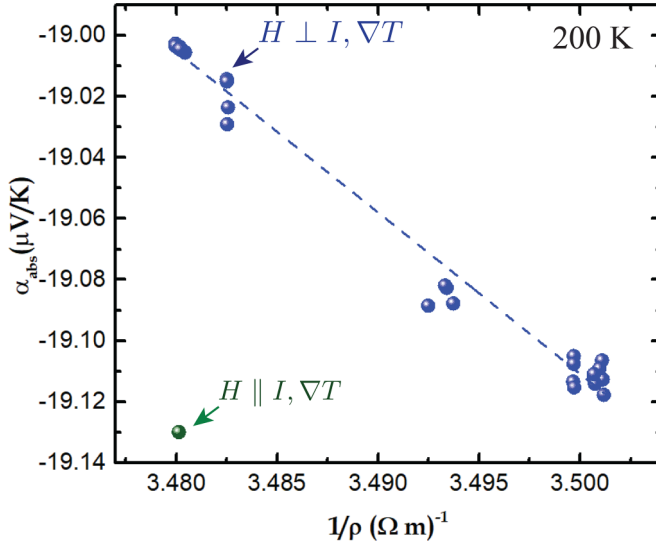
FIG. 8. A representative α_{abs} vs $1/\rho$ plot for the $Co_{25}Fe_{75}$ sample in $-400 < H < 400$ Oe field range in two different applied field directions measured at 200 K. An additional thermopower is present when $H \parallel I$ and ∇T, causing the offset below the linear behavior observed in other metallic ferromagnets. The value of the slope of the line also allows estimation of $[\partial\rho/\partial E]|_{E_F}$ and improved estimation of the electronic diffusion thermopower from Eq. (1).

FIG. 9. Difference in expected and measured values for $\alpha(H, \parallel)$ in low-damping $Co_{25}Fe_{75}$ alloy over temperature range 125–300 K. Inset: Determination of $\Delta\alpha(H, \parallel) = \alpha_{calc}(H, \parallel) - \alpha_{abs}(H, \parallel)$.

we can plausibly explain this pattern by contributions to heat flow from backward volume magnetostatic spin waves formed when $H \parallel \nabla T$, we suggest that this shift in thermopower with applied field direction is a previously unknown form of magnon drag due to this magnetostatic spin wave heat current.

We can quantify this feature by calculating the expected thermopower in the absence of this field-direction dependent magnon drag using similar methods employed for both FM nanowires [45,55] and thin-films [39,42]. In both cases, following the expectations of the Mott relation [Eq. (1)] if $d\rho/dE$ is independent of field strength and orientation, a plot of $\alpha_{abs}(H)$ versus $1/\rho(H)$ (or $1/R(H)$) results in data that falls on a line, with a slope that is proportional to T, fundamental constants and $[\partial\rho/\partial E]|_{E_F}$. In previously reported 3D transition metal alloys and nanowires, this is true for any field orientation. As shown in Fig. 8, this is not the case for the low-damping $Co_{25}Fe_{75}$ film. In this case, data taken with H perpendicular to current and thermal gradient falls on a line as expected, but the values (with saturating field applied) for H parallel to current and field are far below the line. We can define an expected value for the parallel field thermopower, if only electronic effects dominate as previously seen in Ni and Ni-Fe, which we term $\alpha_{calc}(H, \parallel)$. We estimate this value by fitting a line to $\alpha_{abs}(H, \perp)$ versus $1/R(H, \perp)$. From the slope, intercept and measured $1/R(H, \parallel)$ values, we determine $\alpha_{calc}(H, \parallel)$, which provides an estimate for the thermopower for a typical 3D metal alloy in this specific field orientation. The resulting $\alpha_{calc}(H, \parallel)$ versus H is shown in Fig. 5(b), by dottted lines. $\alpha_{calc}(H, \parallel)$ agrees well with typical FM metallic thin films based on the relationship between α and ρ [42]. This clarifies the significant additional negative thermopower added in the low-damping case.
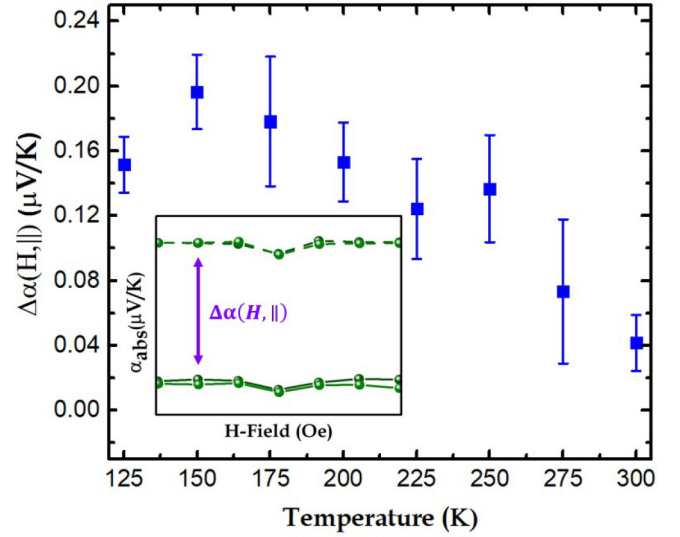
In Fig. 9, we investigate the temperature dependence of $\Delta\alpha(H, \parallel) = \alpha_{calc}(H, \parallel) - \alpha_{abs}(H, \parallel)$. $\Delta\alpha(H, \parallel)$ shows a broad peak between 150–175 K before monotonically decreasing toward 0 as room temperature is approached. In our previous work on field-dependent thermal conductivity on the same thin film samples, we reported a similar temperature dependence [21]. There we presented a simple thermodynamic model and argued that the origin of the field-orientation dependence of k_m stems from two different magnon modes; backward volume spin waves and magnetostatic spin waves which are present here. Given $\alpha_{md} \propto k_m$ from Eq. (2), the resulting $|\alpha(H, \parallel)| > |\alpha(H, \perp)|$ for temperatures below room temperature, corresponds with previous observations of $k(H, \parallel) > k(H, \perp)$. These BVSW modes have much lower population, but relatively high group velocity and long propagation lengths, which we used a very simple model of thermal conductivity in these samples to estimate at ~200 μm [21], and which were measured using spin pumping at 20 GHz in much thinner films to be up to ~20 μm in measurements using Brillouin light scattering [29]. The simple model we employed does not account for diverse spin relaxation processes or other contributions from electron-phonon and magnon-phonon scattering events which could play a role. We also note that the sensitivity of some portion of both k [21] and α_{abs}, as seen in Figs. 5 and 7, to the details of the domain pattern that forms after saturation in different directions is in line with a physical origin of the direction dependence in the relatively long wavelength, long mean free path magnetostatic spin wave modes. The electrons, which dominate the AMR, have much shorter characteristic length scales and are not affected by the different domains in these samples. We hope that this first view into an unusual manifestation of field-direction dependent magnon drag will motivate further study.

We complete our discussion with a more in-depth analysis of the contributions to the zero-field thermopower of this set of films, with the goal of gaining the clearest view of the
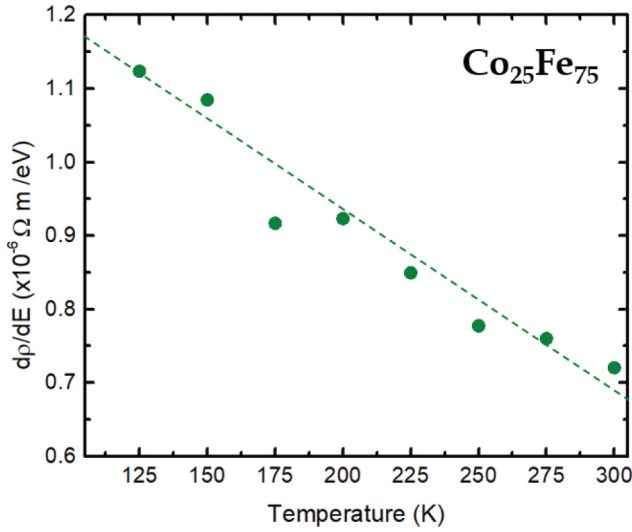
FIG. 10. $[\partial\rho/\partial E]|_{E_F}$ vs T determined for $Co_{25}Fe_{75}$ using the procedure overviewed in the text.

magnon-drag contribution caused by interaction of the field-direction independent, THz frequency thermal magnons with the conduction electrons. As stated earlier, one of the persistent challenges in isolating magnon-drag contributions rests in accurate determination of the electronic diffusion term. While other authors have used the simplest expressions for thermopower of conductors, which may not accurately capture the diffusion term, here we use the magnetic field dependence of the thermopower and resistivity to estimate $[\partial\rho/\partial E]|_{E_F}$ and calculate the electronic diffusion thermopower using the Mott equation. Note again that if $[\partial\rho/\partial E]|_{E_F}$ is independent of magnetic field over the range between 0 and H_{sat}, then diffusion thermopower results in a line (with zero intercept) on a plot of α_{abs} versus $1/\rho$. This is the case for both the $Co_{25}Fe_{75}$ film when $H \perp I$ and ∇T, as shown at 200 K in Fig. 8, and for Ni and Ni-Fe [42]. From the value of the slope, determined from a least squares fit, we then determine the value of $[\partial\rho/\partial E]|_{E_F}$ following Eq. (1). We previously applied this procedure to Ni and Ni-Fe which, perhaps as expected based on relatively similar densities-of-states, have very similar room temperature values of $[\partial\rho/\partial E]|_{E_F}$ of $\sim 4 \times 10^{-7}$ Ωm/eV [39]. Figure 10 plots the $[\partial\rho/\partial E]|_{E_F}$ value versus T for the $Co_{25}Fe_{75}$ film, determined from the slope of $\alpha_{abs}(H)$ versus $1/\rho(H)$ at each T. These values are somewhat higher than we previously reported (only near room temperature) for Ni and Ni-Fe. Note that attempted calculation of $[\partial\rho/\partial E]|_{E_F}$ for $Co_{50}Fe_{50}$ resulted in minimal temperature dependence and very large uncertainty, due to the uncertainty in the field-dependent thermopower.

In Figs. 11(a) and 11(b) we compare the resulting estimate of α_{Mott} to the measured α_{abs} for the Co and $Co_{50}Fe_{50}$ films. We calculate α_{Mott} using measured ρ for each sample. Since for Co and $Co_{50}Fe_{50}$ the MTP values are too small to use the method outlined above or not available, we use a fixed value $\cong 4.7 \times 10^{-7}$ Ωm/eV based on previously measured Ni and Ni-Fe alloy films [39]. For both these films, the estimated diffusion contribution is a relatively close match to the measured thermopower, deviating no more than several
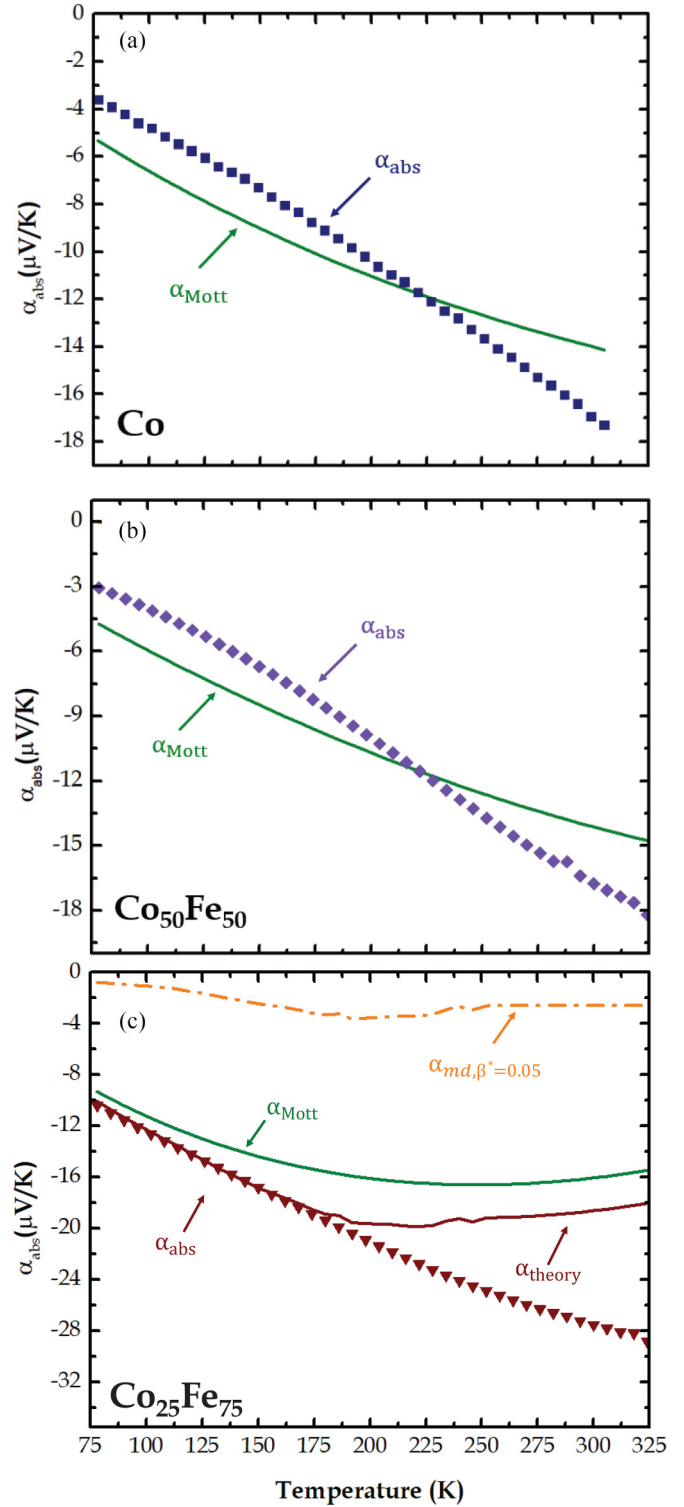

FIG. 11. α_{abs} vs T, over the range 78 to 325 K, of (a) Co thin film (blue symbols) and (b) 75 nm thick $Co_{50}Fe_{50}$, compared to expected electronic diffusion contribution, α_{Mott} (green line), showing similar values at all T. (c) Measured α_{abs} vs T for the $Co_{25}Fe_{75}$ film falls below estimated electronic thermopower at all T, and requires the addition of a magnon-drag contribution, α_{md} (orange line, calculated as described in text). The total theoretical estimate, α_{theory} (maroon line) matches the measured data well below 175 K.

μV/K across this temperature range, suggesting that the thermopower is dominated by electronic diffusion. The situation for the $Co_{25}Fe_{75}$ sample, as shown in Fig. 11(c), is very different. Here the improved estimate of α_{Mott}, which uses the $[\partial\rho/\partial E]|_{E_F}$ value at each T shown in Fig. 10, shows lower (less negative) thermopower at all temperatures, and nearly $5\times$ larger deviation at the higher end of our measured temperature range. This indicates magnon drag is contributing to the thermopower in this low-damping sample.

We can calculate α_{md} following the theory outlined in Eq. (2) using literature values for both the spin polarization, P, and spin stiffness constant, D. P measured for Co-Fe alloys via point contact Andreev reflection measurements and tunneling magnetoresistance measurements gave 0.48 for $Co_{25}Fe_{75}$ [56]. The spin stiffness constant for Co is $D_o \cong 9.28 \times 10^{-40}$ J/m^2 and $D_o \cong 4.48 \times 10^{-40}$ J/m^2 for Fe, both obtained from experimental neutron scattering experiments and extrapolated to zero [57]. For the alloy we compute D based on weighted averages of individual constituents, and interpolate their values over our temperature range of interest given $D = D_o(1 - T/T_c)^\gamma$ where $\gamma = 0.5$ [58]. We estimated T_c for the alloys by averaging bulk T_c values for individual constituents with results agreeing well with micromagnetic calculations [59]. To determine M_s, we first subtract the perpendicular anisotropy from M_s, and use the effective magnetization, M_{eff}. From SQUID magnetometry, we use $M_{eff} \cong 1719$ emu/cm^3 for $Co_{25}Fe_{75}$ [41]. The remaining unknown parameters in Eq. (2) are β^* and k_m. We calculate the magnon heat conductivity, k_m, in Eq. (2) by subtracting the estimated electronic contribution of thermal conductivity, k_e, given by the Wiedemann-Franz law, from the measured thermal conductivity, k_{film} (i.e., $k_m = k_{film} - k_e$), which we previously reported for the same samples discussed here [21]. This k_m peaks near 200 K, and approaches zero near 300 K. Since the values become comparable to expected uncertainty between these temperatures, for this calculation we used a fixed k_m above 250 K. This leaves β^*, which we will adjust as a free parameter, and assume it remains temperature independent for simplicity. Note that the spin transfer torque parameter, β, is usually neglected in transition metals such as Co and Fe, however, theory has shown this contribution can become significant, especially in materials with low Gilbert damping parameters [60,61].

The resulting calculation for $\beta^* = 0.05$ is shown in Fig. 11(c) as the orange line labeled $\alpha_{md,\beta^*=0.05}$. If we take $\alpha_{GD} = 2.1 \times 10^{-3}$ based on earlier measurements [41], this value indicates that $\beta \simeq 0.06$, which is approximately in the range observed in spin torque experiments on Ni-Fe, Co, and Fe thin films [9,62]. Adding this magnon-drag contribution to the α_{Mott} values (here shown in green) gives the total calculated thermopower, α_{calc} shown with the solid maroon line. This curve matches the measured α_{abs} extremely well below $\sim$175 K. At higher temperatures, the combination of magnon-drag theory and electronic diffusion falls below the measured values. This is potentially due to the assumptions made in the theory matching experimental conditions less well as the temperature rises. Similar agreement between theory and experiment only at the lowest T was observed in earlier publications as well [18].
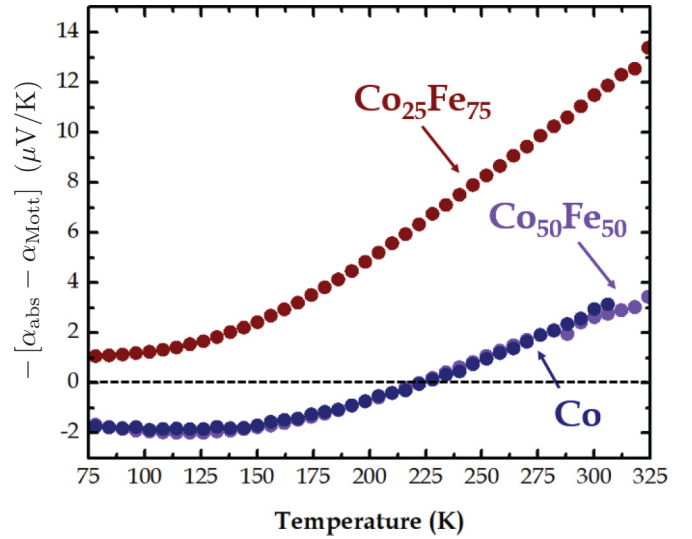

FIG. 12. Estimated nonelectronic thermopower contribution, $-[\alpha_{abs} - \alpha_{Mott}]$ plotted vs T for Co and the two Co-Fe alloy thin films. This suggests that magnon effects could be responsible for more than half the total measured thermopower of the low-damping $Co_{25}Fe_{75}$ sample.

Finally, in Fig. 12 we again highlight the clearest evidence for magnon-drag contributions to thermopower in the low-damping $Co_{25}Fe_{75}$ film by plotting the excess nonelectronic thermopower, $-(\alpha_{abs} - \alpha_{Mott})$ versus T, where both α_{abs} and α_{Mott} are taken from Fig. 11. This shows that both Co and $Co_{50}Fe_{50}$, where typical values of the damping parameter are seen, have small deviations from electronic diffusion thermopower, while the low-damping $Co_{25}Fe_{75}$ film shows significant deviation from purely electronic behavior. Though there is still significant uncertainty on this estimate despite the improved determination of the diffusion contribution that we have made, this curve suggests that the nonelectronic thermopower grows roughly linearly with T in this regime. This is qualitatively consistent with a potential peak in magnon drag above 325 K, which would be in line with expectations from Fe, where the magnon drag peaks near 200 K. The observation of a magnon-drag peak at higher T in $Co_{25}Fe_{75}$ would scale with the higher Curie temperature of this alloy.

Finally, we reiterate that the magnons expected to drive the magnon-drag thermopower we observed in zero field are likely the thermal magnons; magnons with frequencies in the THz that carry average energy comparable to a phonon with temperature near 300 K, which are driven by the strong exchange interaction. We estimated from thermal conductivity that these magnons have mean free paths on order of 1 to a few tens of nanometers in these films. These thermal magnons have larger population, higher velocity, and increased probability of interaction with electrons (due to their shorter wavelength). This leads to larger zero field drag effects, up to 10 μV/K or more, compared to the smaller field-direction dependent effects that rely on the lower energy magnetostatic spin waves discussed earlier that drive shifts in thermopower of only up to 0.2 μV/K.

V. CONCLUSION

In conclusion, our results from field-independent transport measurements and calculations show the spin-transfer torque mechanism of magnon drag can account for an enhanced thermopower if we consider a relatively large magnon-drag thermopower contribution in the polycrystalline alloy with low Gilbert damping parameter, while the Mott relation can describe $Co_{50}Fe_{50}$ well. Through field-dependent measurements reported here, a field-orientation dependent thermopower, when $H \parallel \nabla T$, can be seen in the low-damping $Co_{25}Fe_{75}$, stemming in part from the nonelectronic thermal conductivity described in our previous work. To our knowledge, this is the first observation of this specific type of field-orientation dependent thermopower from magnons in a FM metal. Further experimental and theoretical work is needed to fully explain the underlying physics of these observed field effects.

[1] A. Hoffmann and S. D. Bader, Phys. Rev. Appl. **4**, 047001 (2015).

[2] A. Hirohata, K. Yamada, Y. Nakatani, I.-L. Prejbeanu, B. Diény, P. Pirro, and B. Hillebrands, J. Magn. Magn. Mater. **509**, 166711 (2020).

[3] B. L. Zink, J. Magn. Magn. Mater. **564**, 170120 (2022).

[4] C. H. Back, G. E. W. Bauer, and B. L. Zink, J. Phys. D **52**, 230301 (2019).

[5] K. Vandaele, S. J. Watzman, B. Flebus, A. Prakash, Y. Zheng, S. R. Boona, and J. P. Heremans, Mater. Today Phys. **1**, 39 (2017).

[6] S. R. Boona, R. C. Myers, and J. P. Heremans, Energy Environ. Sci. **7**, 885 (2014).

[7] G. E. W. Bauer, E. Saitoh, and B. J. van Wees, Nat. Mater. **11**, 391 (2012).

[8] G. E. W. Bauer, A. H. MacDonald, and S. Maekawa, Solid State Commun. **150**, 459 (2010).

[9] M. E. Lucassen, C. H. Wong, R. A. Duine, and Y. Tserkovnyak, Appl. Phys. Lett. **99**, 262506 (2011).

[10] D. Miura and A. Sakuma, J. Phys. Soc. Jpn. **81**, 113602 (2012).

[11] S. Hoffman, K. Sato, and Y. Tserkovnyak, Phys. Rev. B **88**, 064408 (2013).

[12] F. Körmann, B. Grabowski, B. Dutta, T. Hickel, L. Mauger, B. Fultz, and J. Neugebauer, Phys. Rev. Lett. **113**, 165503 (2014).

[13] B. Flebus, R. A. Duine, and Y. Tserkovnyak, Europhys. Lett. **115**, 57004 (2016).

[14] M. Beens, J. P. Heremans, Y. Tserkovnyak, and R. A. Duine, J. Phys. D **51**, 394002 (2018).

[15] M. M. H. Polash, H. Polash, F. Mohaddes, M. Rasoulianboroujeni, and D. Vashaee, J. Mater. Chem. C **8**, 4049 (2020).

[16] S. Nikolov, J. Tranchida, K. Ramakrishna, M. Lokamani, A. Cangi, and M. A. Wood, J. Mater. Sci. **57**, 10535 (2022).

[17] M. V. Costache, G. Bridoux, I. Neumann, and S. O. Valenzuela, Nat. Mater. **11**, 199 (2012).

[18] S. J. Watzman, R. A. Duine, Y. Tserkovnyak, S. R. Boona, H. Jin, A. Prakash, Y. Zheng, and J. P. Heremans, Phys. Rev. B **94**, 144407 (2016).

[19] S. Srichandan, S. Wimmer, S. Pöllath, M. Kronseder, H. Ebert, C. H. Back, and C. Strunk, Phys. Rev. B **98**, 020406(R) (2018).

[20] Y. Zheng, E. J. Weiss, N. Antolin, W. Windl, and J. P. Heremans, J. Appl. Phys. **126**, 125107 (2019).

[21] M. R. Natale, D. J. Wesenberg, E. R. J. Edwards, H. T. Nembach, J. M. Shaw, and B. L. Zink, Phys. Rev. Mater. **5**, L111401 (2021).

[22] A. A. Serga, A. V. Chumak, and B. Hillebrands, J. Phys. D **43**, 264002 (2010).

[23] A. D. Karenowska, A. V. Chumak, A. A. Serga, and B. Hillebrands, in *Handbook of Spintronics* (Springer, Netherlands, 2016), pp. 1505–1549.

[24] R. Weber, D.-S. Han, I. Boventer, S. Jaiswal, R. Lebrun, G. Jakob, and M. Kläui, J. Phys. D **52**, 325001 (2019).

[25] H. S. Körner, M. A. W. Schoen, T. Mayer, M. M. Decker, J. Stigloher, T. Weindler, T. N. G. Meier, M. Kronseder, and C. H. Back, Appl. Phys. Lett. **111**, 132406 (2017).

[26] R. Douglass, Phys. Rev. **129**, 1132 (1963).

[27] D. Sun, E. Ehrenfreund, and Z. V. Vardeny, Analyst **50**, 1781 (2014).

[28] S. R. Boona and J. P. Heremans, Phys. Rev. B **90**, 064421 (2014).

[29] L. Flacke, L. Liensberger, M. Althammer, H. Huebl, S. Geprägs, K. Schultheiss, A. Buzdakov, T. Hula, H. Schultheiss, E. R. J. Edwards, H. T. Nembach, J. M. Shaw, R. Gross, and M. Weiler, Appl. Phys. Lett. **115**, 122402 (2019).

[30] P. Wessels, A. Vogel, J. N. Tödt, M. Wieland, G. Meier, and M. Drescher, Sci. Rep. **6**, 22117 (2016).

[31] U. K. Bhaskar, G. Talmelli, F. Ciubotaru, C. Adelmann, and T. Devolder, J. Appl. Phys. **127**, 033902 (2020).

[32] S. J. Mason, A. Hojem, D. J. Wesenberg, A. D. Avery, and B. L. Zink, J. Appl. Phys. **127**, 085101 (2020).

[33] M. Jonson and G. D. Mahan, Phys. Rev. B **21**, 4223 (1980).

[34] A. D. Avery, R. Sultan, D. Bassett, D. Wei, and B. L. Zink, Phys. Rev. B **83**, 100401(R) (2011).

[35] F. J. Blatt, D. J. Flood, V. Rowe, P. A. Schroeder, and J. E. Cox, Phys. Rev. Lett. **18**, 395 (1967).

[36] G. N. Grannemann and L. Berger, Phys. Rev. B **13**, 2072 (1976).

[37] B. H. Kim, J. S. Kim, T. H. Park, D. S. Lee, and Y. W. Park, J. Appl. Phys. **103**, 113717 (2008).

[38] R. Sultan, A. D. Avery, G. Stiehl, and B. L. Zink, J. Appl. Phys. **105**, 043501 (2009).

[39] D. Wesenberg, A. Hojem, R. K. Bennet, and B. L. Zink, J. Phys. D **51**, 244005 (2018).

[40] M. T. Kief and W. F. Egelhoff, Phys. Rev. B **47**, 10785 (1993).

[41] M. A. W. Schoen, D. Thonig, M. L. Schneider, T. J. Silva, H. T. Nembach, O. Eriksson, O. Karis, and J. M. Shaw, Nat. Phys. **12**, 839 (2016).

[42] A. D. Avery, M. R. Pufall, and B. L. Zink, Phys. Rev. B **86**, 184408 (2012).

[43] A. D. Avery and B. L. Zink, Phys. Rev. Lett. **111**, 126602 (2013).

[44] T. R. McGuire and R. I. Potter, IEEE Trans. Magn. **11**, 1018 (1975).

[45] T. Böhnert, V. Vega, A.-K. Michel, V. M. Prida, and K. Nielsch, Appl. Phys. Lett. **103**, 092407 (2013).

[46] J. Pelzl, R. Meckenstock, D. Spoddig, F. Schreiber, J. Pflaum, and Z. Frait, J. Phys.: Condens. Matter **15**, S451 (2003).

[47] T. Böhnert, A. C. Niemann, A.-K. Michel, S. Bäßler, J. Gooth, B. G. Tóth, K. Neuróhr, L. Péter, I. Bakonyi, V. Vega, V. M. Prida, and K. Nielsch, Phys. Rev. B **90**, 165416 (2014).

[48] N. Marchal, T. da Câmara Santa Clara Gomes, F. Abreu Araujo, and L. Piraux, Nanoscale Res. Lett. **15**, 137 (2020).

[49] Note that a true swept-field experiment is difficult or impossible using our technique, which employs a relatively massive copper sample mount and radiation shield to maintain a well-controlled thermal gradient. A changing field drives eddy currents in the copper that changes the temperature during a field sweep. Here we always stabilize the field before measuring any thermovoltage.

[50] A. D. Kent, U. Rüdiger, J. Yu, L. Thomas, and S. S. P. Parkin, J. Appl. Phys. **85**, 5243 (1999).

[51] A. Kent, U. Ruediger, J. Yu, S. Zhang, P. Levy, Y. Zhong, and S. Parkin, IEEE Trans. Magn. **34**, 900 (1998).

[52] U. Ruediger, J. Yu, S. Zhang, A. D. Kent, and S. S. P. Parkin, Phys. Rev. Lett. **80**, 5639 (1998).

[53] L. Wang, R. Y. Zhang, X. J. Wang, W. T. Xu, W. L. Zhao, G. Li, and Y. F. Liu, Mater. Res. Express **5**, 016411 (2018).

[54] M. Bolte, M. Steiner, C. Pels, M. Barthelmeß, J. Kruse, U. Merkt, G. Meier, M. Holz, and D. Pfannkuche, Phys. Rev. B **72**, 224436 (2005).

[55] V. D. Nguyen, C. Naylor, L. Vila, A. Marty, P. Laczkowski, C. Beigné, L. Notin, Z. Ishaque, and J. P. Attané, Appl. Phys. Lett. **99**, 262504 (2011).

[56] S. V. Karthik, T. M. Nakatani, A. Rajanikanth, Y. K. Takahashi, and K. Hono, J. Appl. Phys. **105**, 07C916 (2009).

[57] M. Pajda, J. Kudrnovský, I. Turek, V. Drchal, and P. Bruno, Phys. Rev. B **64**, 174402 (2001).

[58] K. Niitsu, J. Phys. D **53**, 39LT01 (2020).

[59] L. Rohman, A. Arkundato, Y. T. Mulyani, and D. Djuhana, J. Phys.: Conf. Ser. **1825**, 012003 (2021).

[60] K. Gilmore, I. Garate, A. H. MacDonald, and M. D. Stiles, Phys. Rev. B **84**, 224412 (2011).

[61] S. Zhang and Z. Li, Phys. Rev. Lett. **93**, 127204 (2004).

[62] L. Heyne, J. Rhensius, D. Ilgaz, A. Bisig, U. Rüdiger, M. Kläui, L. Joly, F. Nolting, L. J. Heyderman, J. U. Thiele, and F. Kronast, Phys. Rev. Lett. **105**, 187203 (2010).